J. Fluid Mech. (1990), *vol.* 216, *pp.* 285–298
Printed in Great Britain

Natural convection in porous media: effect of weak dispersion on bifurcation

By XIAOWEI S. HE AND JOHN G. GEORGIADIS
Department of Mechanical Engineering and Materials Science, Duke University, Durham, NC 27706, USA

(Received 4 August 1989 and in revised form 13 December 1989)

We use weakly nonlinear analysis via a two-parameter expansion to study bifurcation of conduction into cellular convection of an internally heated fluid in a porous medium that forms a horizontal layer between two isothermal walls. The Darcy–Boussinesq model of convection is enhanced by including two nonlinear terms: (i) quadratic (Forchheimer) drag; and (ii) hydrodynamic dispersion enhancement of the thermal conductivity described by a weak linear relationship between effective conductivity and local amplitude of filtration velocity. The impact of the second term on the shape of the bifurcation curve for two-dimensional rolls is profound in the presence of uniform volumetric heating. The resulting bifurcation structure is unlike any pitchfork bifurcations typical of the classical Bénard problem. Although direct experimental validation of the novel bifurcation is not available, we would like to register it as an alternative or a supplement to models of small imperfections, and as an attempt to account for the scatter of observed critical values for the first bifurcation.

1. Introduction

Studies of buoyancy-driven convection in fully saturated porous media are abundant in the fluid mechanics/heat transfer literature but they are also limited in scope. Although the porous medium typically consists of two components (a solid matrix saturated by a fluid phase), the majority of mathematical models treat it as a continuum. This simplification requires the definition of 'effective' transport properties that are usually assumed to be constant, i.e. independent of the flow parameters. For example, an effective conductivity that depends on geometrical properties and the conductivities of the individual phases is assigned to a fluid-saturated porous medium. We shall refer to these as Darcian formulations. Only recently have non-Darcian models been implemented; Rubin (1974) was the first author to study instabilities in the presence of (hydrodynamic) dispersion effects in mixed convection in porous media. Despite the fact that effective transport coefficients have been shown to depend on the local filtration velocity for disordered (Koch & Brady 1985; Georgiadis & Catton 1988*a*) and ordered media (Levec & Carbonell 1985; Koch *et al.* 1989), this dependence has been neglected *a priori* in natural convection flows. Notable exceptions are the studies by Neischloss & Dagan (1975), Kvernvold & Tyvand (1980), and Georgiadis & Catton (1988*b*) of the Bénard problem in porous media. This mathematical problem concerns the stability of a horizontal layer of fluid in a porous medium subject to a vertical temperature gradient and it can be mapped onto a variety of physical problems.

In horizontally unbounded porous layers that are confined between two impermeable walls and heated isothermally from below (refer to figure 1), the onset of convection (first bifurcation) takes place in the form of two-dimensional rolls with the following critical parameters (λ is the wavelength equal to the width of two counter-rotating rolls and L is the layer thickness):

$$Ra_{\mathrm{m}}^{\mathrm{crit}} = 4\pi^2, \quad \lambda^{\mathrm{crit}} = \frac{2\pi}{\alpha^{\mathrm{crit}}} = 2L, \tag{1}$$

where Ra_{m} is the porous-medium Rayleigh number. As it will become obvious in the following section, this Rayleigh number is based on two lengthscales: a macroscopic length, L, and a microscopic length (the square root of the permeability, proportional to the pore size or bead diameter, d).

Kvernvold & Tyvand (1980) incorporated a quadratic dispersion term in the energy equation and modified the linear stability regime for two-dimensional convection. Georgiadis & Catton (1988*b*) used a linear hydrodynamic dispersion model to study finite-amplitude convection in the porous-medium Bénard problem. Although two different models were used, the onset of convection proved to be independent of the dispersive effect in both cases. Experiments on ordered packed beds by Katto & Masuoka (1967) and Close, Symmons & White (1985) have verified that the first critical Rayleigh number, (1), remains constant regardless of the bead diameter/layer thickness ratio (d/L) of the packed beds (which affects the magnitude of the dispersive term). Such results seem to justify neglecting the dispersive effect in the study of the onset of convection in the porous Bénard problem.

However, the experimental evidence of natural convection in an internally heated fluid in a porous layer exhibits a peculiar scatter near the onset of convection. A series of experimental investigations in particulate beds confined between an isothermal upper surface and an adiabatic lower wall have been conducted by Buretta & Berman (1976); Hardee & Nilson (1977); Rhee, Dhir & Catton (1978); and Kulacki & Freeman (1979). The measured critical Rayleigh numbers (based on the volumetric heat generation rate) are scattered within a 39% interval above the theoretical estimate given by Buretta & Berman (1976) based on Darcian model. Rhee *et al.* (1978) hypothesized that this discrepancy is caused by the non-uniformity of the thermal field induced by inductively heating heterogeneous media with much different thermal conductivities (steel beads in water).

We offer herein an alternative hypothesis which can explain the scatter in critical parameters. We propose a bifurcation analysis of the porous-medium Bénard problem with internal heating that will account for non-Darcian effects according to equations (2)–(4) of the next section. We try a double expansion in terms of the classical bifurcation parameter ϵ and the dispersivity δ (which is proportional to d/L according to equation (6)) and then follow the procedure outlined in Section 76 of the monograph by Joseph (1976).

Our results show that the effect of dispersion on natural convection in this case is fundamentally different from the case without internal heat generation. In the latter case, the relative importance of dispersion is expressed by the particle Péclet number (based on d) which is low for a wide range of Rayleigh numbers above the critical, cf. Kvernvold & Tyvand (1980); Georgiadis & Catton (1988*b*). Furthermore, this work serves to suggest that non-Darcian natural convection models no longer be ignored (in the name of simplicity or mathematical tractability).

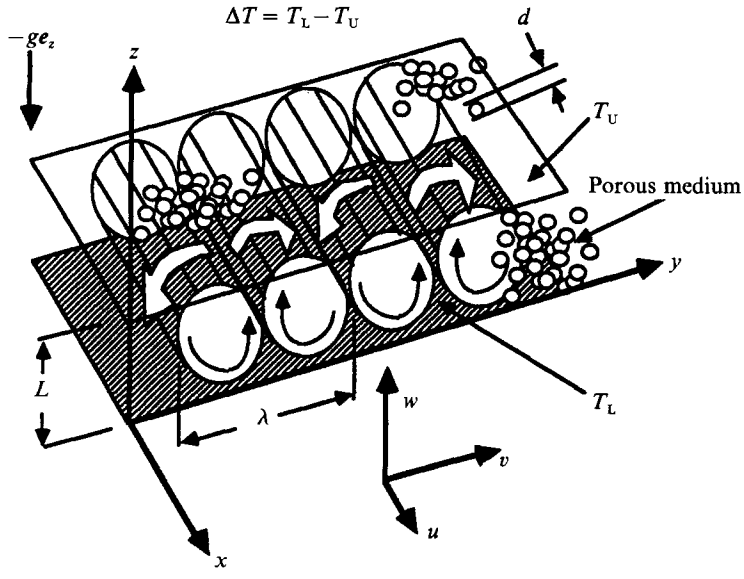

FIGURE 1. The porous-medium Bénard problem. Schematic of the two-dimensional cellular wave pattern.

2. Mathematical formulation

We consider buoyancy-driven flow in a fluid-saturated porous medium confined between two parallel horizontal plates, as shown in figure 1. The medium is characterized by its uniform porosity ϕ, permeability, γ, inertial resistance coefficient b, and stagnant thermal diffusivity $a_m = k_m/(\rho c)_f$; k_m is the effective stagnant conductivity of the medium, ν is the kinematic viscosity, and $(\rho c)_f$ is the thermal capacity of the fluid. The medium is internally heated from distributed heat sources of strength Q. By non-dimensionalizing lengths, velocities, pressure, and temperature with L, a_m/L, $\rho\nu a_m/L^2$, and $\Delta T = T_L - T_U$, respectively, the following governing equations and boundary conditions for the locally averaged (Darcy) velocity V and temperature T are obtained:

$$\nabla \cdot V = 0, \tag{2}$$

$$\frac{1}{\phi Pr_m}\frac{\partial V}{\partial t} = -\nabla P + \frac{Ra_m}{Da} T e_z - \frac{1}{Da} V - \omega |V| V, \tag{3}$$

$$\frac{(\rho c)_m}{(\rho c)_f}\frac{\partial T}{\partial t} = -V \cdot \nabla T + \nabla \cdot [(1 + \boldsymbol{D}^*) \nabla T] + \frac{Ra_1}{|Ra_m|}, \tag{4}$$

$$V \cdot e_z = 0 \quad \text{and} \quad T = 1 - z \quad \text{at} \quad z = 0, 1, \tag{5}$$

where $Ra_m = g\beta\Delta T\gamma L/(\nu a_m)$ is the (porous) external Rayleigh number, $Da = \gamma/L^2$ is the Darcy number, and $Ra_1 = Ra_m Q L^2/(k_m \Delta T)$ is the internal Rayleigh number. t is the time and e_z denotes the unit vector in the z-direction (vertical).

In the equations above, P is the local interstitial fluid pressure minus the hydrostatic component, and T is the local (average) temperature minus the upper wall temperature T_U. The relative importance of the inertial (Forchheimer) quadratic drag term in (3) is given by the magnitude of $\omega = bL/\gamma Pr_m$, where the porous medium Prandtl number is defined as $Pr_m = \nu/a_m$. The standard Boussinesq approximation is made in the derivation of (2)–(4); its validity has been supported

by the work of Gartling & Hickox (1985). The momentum equation (3), which was supported on empirical basis by Ergun (1952), was derived by Georgiadis & Catton (1987) on the basis of a microscopic stochastic model of randomly packed beds. The slip conditions at the walls are consistent with the absence of Brinkman's correction in the momentum equation (3).

Georgiadis & Catton (1988*a*) also supported the derivation of the energy equation (4) on the basis of the interstitial hydrodynamic field statistics in disordered media. It is assumed that the temperature of the fluid and solid phases are 'locally' equal; this is known as the 'local thermal equilibrium' assumption. The tensor $\boldsymbol{D}^*$ on the right-hand side of (4) accounts for the enhancement of heat transport due to dispersion and has been taken by Georgiadis & Catton (1988*a*) to be isotropic. The ratio of dispersive to stagnant conductivity is given by

$$\tfrac{1}{3}\,\text{Trace}\,\{\boldsymbol{D}^*\} = \left(\frac{C}{1-\phi}\frac{d}{L}|\boldsymbol{V}|\right) = \delta|\boldsymbol{V}| \tag{6}$$

where $\delta = Cd/(1-\phi)L$ is the dispersivity. Notice that this parameter depends only on the ratio d/L which is a measure of the coarseness of the packed bed (d represents the characteristic dimension of the pores or beads); $\delta \ll 1$ for most practical cases. The coefficient C depends on the statistics of the microstructure of the medium; Georgiadis & Catton (1988*b*) used the value $C = 0.36$.

The base (equilibrium) state of (2)–(5) is given by the pure heat conduction through the layer:

$$\boldsymbol{V}_{\rm b} = 0, \tag{7}$$

$$T_{\rm b} = -\tfrac{1}{2}\eta z^2 + (\tfrac{1}{2}\eta - 1)\,z + 1 \quad \text{where} \quad \eta = Ra_{\rm I}/|Ra_{\rm m}|. \tag{8}$$

After considering a perturbation $(\boldsymbol{U}, \theta)$ on the base state $(\boldsymbol{V}_{\rm b}, T_{\rm b})$,

$$\boldsymbol{V} = \boldsymbol{V}_{\rm b} + \boldsymbol{U} \quad \text{and} \quad T = T_{\rm b} + \frac{\theta}{R}, \quad \text{with} \quad R = |Ra_{\rm m}|^{\frac{1}{2}}, \tag{9}$$

equations (2)–(4) and the boundary conditions (5) become

$$\boldsymbol{\nabla}\cdot\boldsymbol{U} = 0, \tag{10}$$

$$\frac{Da}{\phi Pr_{\rm m}}\frac{\partial \boldsymbol{U}}{\partial t} = -Da\,\boldsymbol{\nabla}P \pm R\theta\boldsymbol{e}_z - \boldsymbol{U} - \omega Da|\boldsymbol{U}|\,\boldsymbol{U}, \tag{11}$$

$$\frac{(\rho c)_{\rm m}}{(\rho c)_{\rm f}}\frac{\partial\theta}{\partial t} = -\boldsymbol{U}\cdot\boldsymbol{\nabla}\theta + RwG(z) + \nabla^2\theta + \delta\boldsymbol{\nabla}\cdot(|\boldsymbol{U}|\,\boldsymbol{\nabla}\theta) - R\delta\boldsymbol{\nabla}\cdot(|\boldsymbol{U}|\,G(z)\,\boldsymbol{e}_z), \tag{12}$$

$$\boldsymbol{U}\cdot\boldsymbol{e}_z = \theta = 0, \tag{13}$$

where w is the vertical component of the perturbation velocity $\boldsymbol{U}$. The vertical base temperature gradient is defined as follows:

$$G(z) = -\boldsymbol{e}_z\cdot\boldsymbol{\nabla}T_{\rm b} = \eta z - \tfrac{1}{2}\eta + 1. \tag{14}$$

The double sign $\pm$ in front of the modified Rayleigh number R in (11) corresponds to $+$ if the lower surface is hotter than the upper, $T_{\rm U} > T_{\rm L}$ and $-$ if $T_{\rm U} < T_{\rm L}$. This convention is kept throughout this work.

Since there is no external rotation or magnetic field, we assume that the principle of exchange of stabilities holds for the spectral problem for disturbances proportional to $e^{-\sigma t}$. Therefore, $\sigma(R)$ is real valued, and the condition for marginal stability is

given by $\sigma = 0$. The weakly nonlinear stationary solution of (10)–(13) can be found by expanding the pressure P, and the quantity $\boldsymbol{q}$, which represents the four-component perturbation vector $(\boldsymbol{U}, \theta)$, into a double Taylor series in terms of the parameters ϵ and δ:

$$\boldsymbol{q} = \epsilon \boldsymbol{q}_0 + \epsilon^2 \boldsymbol{q}_1 + \epsilon\delta \boldsymbol{q}_2 + o(\epsilon^2, \epsilon\delta). \tag{15}$$

The same expansion is carried out for the modified Rayleigh number:

$$R = R_0 + \epsilon R_1 + \delta R_2 + o(\epsilon, \delta). \tag{16}$$

After substituting the expansions (15) and (16) into (10)–(12) and collecting the coefficients up to orders ϵ, ϵ^2, and $\epsilon\delta$, the resulting equations for each order can be written in matrix form:

$O(\epsilon)$

$$\left.\begin{aligned} &\boldsymbol{D}^{\mathrm{T}} \cdot \boldsymbol{q}_0 = 0, \\ &\boldsymbol{L}_{00} \cdot \boldsymbol{q}_0 = \boldsymbol{D} P_0, \end{aligned}\right\} \tag{17}$$

$O(\epsilon^2)$

$$\left.\begin{aligned} &\boldsymbol{D}^{\mathrm{T}} \cdot \boldsymbol{q}_1 = 0, \\ &\boldsymbol{L}_{00} \cdot \boldsymbol{q}_1 + \boldsymbol{L}_{10} \cdot \boldsymbol{q}_0 + \boldsymbol{M}_{00} \cdot \boldsymbol{q}_0 + \boldsymbol{N}_{00} \cdot \boldsymbol{q}_0 = \boldsymbol{D} P_1. \end{aligned}\right\} \tag{18}$$

$O(\epsilon\delta)$

$$\left.\begin{aligned} &\boldsymbol{D}^{\mathrm{T}} \cdot \boldsymbol{q}_2 = 0, \\ &\boldsymbol{L}_{00} \cdot \boldsymbol{q}_2 + \boldsymbol{L}_{20} \cdot \boldsymbol{q}_0 + \boldsymbol{F}_{00} \cdot \boldsymbol{I} = \boldsymbol{D} P_2, \end{aligned}\right\} \tag{19}$$

where $\boldsymbol{D}^{\mathrm{T}}$, $\boldsymbol{q}_i$, $\boldsymbol{I}$, $\boldsymbol{L}_{00}$, $\boldsymbol{L}_{10}$, $\boldsymbol{L}_{20}$, $\boldsymbol{M}_{00}$, $\boldsymbol{N}_{00}$ and $\boldsymbol{F}_{00}$ are given in Appendix A.

The solution of the problem (17) delineates the stability domain of the conductive base state (7), (8) to infinitesimal disturbances without the effect of dispersion. This reference stability domain is described by the relationship $R_0 = R_0(\eta)$. Since Gasser & Kazimi (1976) have computed the above relationship for the Brinkman-extended Darcy model, comparison with our results will help assess the validity of the momentum equation (3). By inspecting the nonlinear operators given in Appendix A, we can see that (18) gives the effect of the nonlinear drag (Forchheimer term) of (3), while (19) gives the influence of dispersivity, δ, near the first bifurcation.

3. Solution of the linear problem

By eliminating the horizontal components of velocity and P_0 from the system (17), we obtain the equivalent system

$$-\nabla^2 w_0 \pm R_0 \nabla_1^2 \theta_0 = 0, \tag{20}$$

$$R_0 G(z)\, w_0 + \nabla^2 \theta_0 = 0, \tag{21}$$

where $$\nabla^2 = \frac{\partial^2}{\partial x^2} + \frac{\partial^2}{\partial y^2} + \frac{\partial^2}{\partial z^2}, \quad \nabla_1^2 = \frac{\partial^2}{\partial x^2} + \frac{\partial^2}{\partial y^2}.$$

The solution of system (20), (21) subject to homogeneous boundary conditions can be obtained with separation of variables

$$\begin{bmatrix} w_0 \\ \theta_0 \end{bmatrix} = \begin{bmatrix} W_0(z) \\ \Theta_0(z) \end{bmatrix} \Phi(x, y), \tag{22}$$

where $\Phi(x, y)$ is the planform function satisfying a Helmholtz equation

$$\nabla_1^2 \Phi(x, y) = -\alpha^2 \Phi(x, y). \tag{23}$$

Φ is an eigenfunction of (23) with eigenvalue α (horizontal wavenumber). Substituting (22) and (23) into (20) and (21), we obtain

$$(D^2-\alpha^2)\,W_0 \pm R_0\,\alpha^2\Theta_0 = 0, \tag{24}$$

$$R_0\,G(z)\,W_0 + (D^2-\alpha^2)\,\Theta_0 = 0, \tag{25}$$

where $D = d/dz$, $D^2 = d^2/dz^2$. The boundary conditions associated with (24) and (25) are homogeneous ($W_0 = \Theta_0 = 0$ at $z = 0, 1$). Since $G(z)$ is positive for $0 < z < 1$, every eigenvalue $R_0(\alpha)$ is a simple eigenvalue of (24) and (25), cf. Joseph (1976, Appendix D, Vol. 1).

We employ the standard Galerkin method to solve the eigenvalue problem (24), (25). The following Fourier series expansion is introduced:

$$\Theta_0(z) = \frac{1}{\alpha^2}\sum_{m=1}^{N} A_m \sin(m\pi z) \tag{26}$$

Equation (24) thus becomes

$$(D^2-a^2)\,W_0 \pm R_0 \sum_{m=1}^{N} A_m \sin(m\pi z) = 0. \tag{27}$$

The particular solution of (27) is given by

$$W_0(z) = \sum_{m=1}^{N} B_m \sin(m\pi z), \tag{28}$$

where

$$B_m = \frac{\pm R_0 A_m}{m^2\pi^2+\alpha^2}. \tag{29}$$

It is easy to show that (28) is also the general solution of (27). We then substitute (26) and (28) back into (25) to obtain the following algebraic equation:

$$\sum_{m=1}^{N}\left[\frac{\pm R_0^2\,G(z)}{m^2\pi^2+\alpha^2} - \left(\frac{m^2\pi^2}{\alpha^2}+1\right)\right] A_m \sin(m\pi z) = 0. \tag{30}$$

By multiplying (30) by $\sin(n\pi z)$ and integrating between $z = 0$ and $z = 1$, we obtain a set of N equations:

$$\sum_{m=1}^{N}\left[\frac{\pm R_0^2\,G(z)}{m^2\pi^2+\alpha^2} I_0^{mn} - \left(\frac{m^2\pi^2}{\alpha^2}+1\right) I_1^{mn}\right] A_m = 0, \quad n = 1, 2, \ldots, N. \tag{31}$$

The integrals I_0^{mn} and I_1^{mn} are given in Appendix A.

We first solve the eigenvalue problem (31) for a wide range of α with η as a parameter. In order for A_m to be the non-trivial solution, the determinant of the coefficient matrix has to vanish; an analytic expression for $R_0(\alpha)$ is derived and we isolate only the positive $R_0(\alpha)$ roots. All the algebra and root finding is performed with the symbolic manipulation program MAPLE on a SUN 4 computer. The neutral curves for the unstably and stably heated layers are given in figure 2(*a*). To determine the necessary truncation level N, we used two-, three-, and four-term Galerkin expansions and compared the $R_0(\alpha)$ result in figure 2(*b*). It is obvious that $N = 3$ provides an adequate level of accuracy.

The critical values are given by the minimum positive eigenvalue $R_0(\alpha)$; this minimum was found analytically with MAPLE by solving the equation $dR_0(\alpha)/d\alpha = 0$. A tabulation of the results is presented in tables 1 and 2 (recall that $Ra_1 = \eta|Ra_m|$,

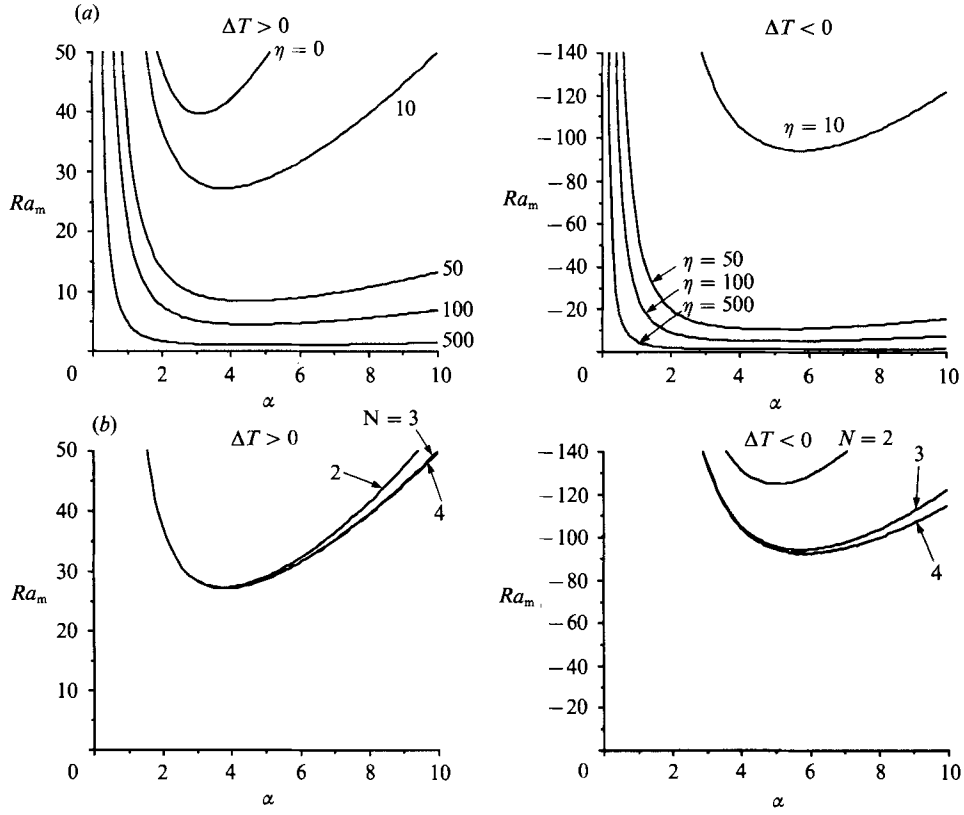

FIGURE 2. Plots of the external Rayleigh number Ra_m vs. the horizontal wavenumber α. (*a*) Effect of the internal heat generation parameter η. (*b*) Effect of truncation level of the Galerkin expansion N at $\eta = 10$.

		Ra_m^{crit}		
η	α^{crit}	Present	Hwang	Ra_I^{crit}
0	3.14	39.48	39.48	0
10	3.81	27.02	27.02	270.22
20	4.19	17.64	17.63	352.73
30	4.34	12.92	12.91	387.65
40	4.42	10.17	10.16	406.81
60	4.50	7.12	7.11	427.20
80	4.53	5.47	5.47	437.90
100	4.56	4.44	4.44	444.49
500	4.64	0.93		466.45
1000	4.65	0.47		469.31

TABLE 1. Tabulation of the values of the neutral curve, for unstably heated layer, $\Delta T > 0$ (three-term approximation). Comparison with results by Hwang (1971).

by definition). Our results agree within roundoff error with the critical (1) in the case of zero heat generation ($\eta = Ra_I = 0$). A plot of the stability curves is shown in the composite figure 3. It contains two curves: the one marked + corresponds to the case $T_L > T_U$ (unstably heated layer), the − corresponds to $T_L < T_U$. Of course, the sign of Ra_m in the latter case is negative.

η	α^{crit}	$Ra_{\text{m}}^{\text{crit}}$	$Ra_{\text{I}}^{\text{crit}}$
10	5.72	−94.05	940.55
20	5.18	−32.56	651.13
30	5.00	−19.42	582.62
40	4.92	−13.80	552.01
60	4.83	−8.73	523.53
80	4.79	−6.38	510.02
100	4.76	−5.02	502.14
500	4.68	−0.96	477.97
1000	4.67	−0.48	475.03

TABLE 2. Tabulation of the values of the neutral curve for stably heated layer, $\Delta T < 0$ (three-term approximation)

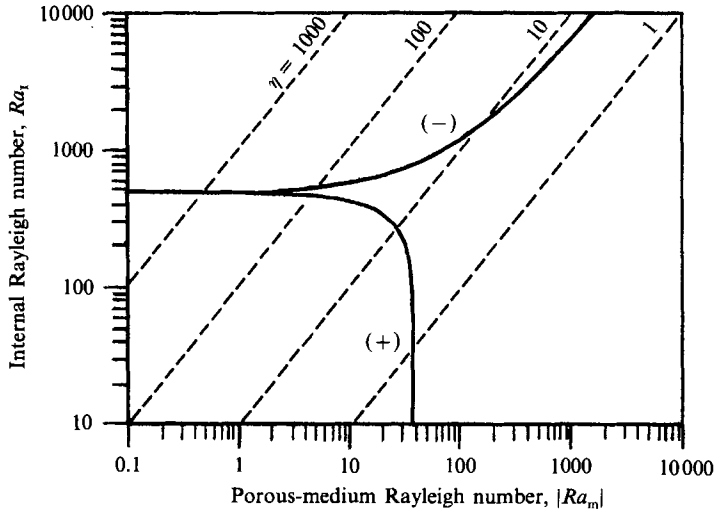

FIGURE 3. Plot of stability curves for the porous-medium Bénard problem with internal heat generation. Notation: (+) heating from below, $\Delta T > 0$; (−) heating from above, $\Delta T < 0$.

We can compare our critical values with the data of Hwang (1971) (see table 1), and Gasser & Kazimi (1976) obtained with a Brinkman-extended model. Although free-rigid boundary conditions were used in the above studies, they agree well with our results obtained for slip boundary conditions, as shown in table 1. The convergence of the Brinkman critical values to these given by the Darcy model occurs for small values of the Darcy number, $Da < 10^{-3}$ (Rudraiah, Veerappa & Balachandra 1982; Selimos & Poulikakos 1985).

Following the estimation of the critical parameters, we can find the eigenfunction vector $\boldsymbol{q}_0$. We choose to restrict our analysis to two-dimensional convection. Starting with a sinusoidal planform Φ, we compute v_0, w_0, and θ_0 from (17) and give the results in Appendix A, (A 3)–(A 6). Two-dimensional rolls have indeed been shown to be a stable bifurcation solution for weakly supercritical convection.

4. Bifurcation curve

The nonlinear problems (18) and (19) produce R_1 and R_2, respectively, and thus give the shape of the bifurcation curve in the vicinity of R_0. Since $R_0(\alpha)$ is a simple eigenvalue of (17), the systems (18) and (19) are solvable if

$$\langle \boldsymbol{q}_0^* \cdot \boldsymbol{L}_{10} \cdot \boldsymbol{q}_0 \rangle + \langle \boldsymbol{q}_0^* \cdot \boldsymbol{M}_{00} \cdot \boldsymbol{q}_0 \rangle + \langle \boldsymbol{q}_0^* \cdot \boldsymbol{N}_{00} \cdot \boldsymbol{q}_0 \rangle = 0, \tag{32}$$

$$\langle \boldsymbol{q}_0^* \cdot \boldsymbol{L}_{20} \cdot \boldsymbol{q}_0 \rangle + \langle \boldsymbol{q}_0^* \cdot \boldsymbol{F}_{00} \cdot \boldsymbol{I}_0 \rangle = 0, \tag{33}$$

where $\langle \cdot \rangle$ denotes volume integral over flow field, and $\boldsymbol{q}_0^*$ is the adjoint eigenfunction of (B 1) and (B 2) in Appendix B corresponding to the linear problem (17). The solvability conditions (32) and (33) yield the following relations for $R_1(\boldsymbol{q}_0)$ and $R_2(\boldsymbol{q}_0)$:

$$-R_1 \langle \pm w_0^* \theta_0 + G(z)\, \theta_0^*\, w_0 \rangle + \frac{|\epsilon|}{\epsilon} \omega Da \langle \boldsymbol{U}_0^* \cdot \boldsymbol{U}_0 |\boldsymbol{U}_0| \rangle + \langle \theta_0^* (\boldsymbol{U}_0 \cdot \nabla) \theta_0 \rangle = 0, \tag{34}$$

$$-R_2 \langle \pm w_0^* \theta_0 + G(z)\, \theta_0^*\, w_0 \rangle + \frac{|\epsilon|}{\epsilon} R_0 \left\langle \theta_0^* \frac{\partial}{\partial z} |\boldsymbol{U}_0|\, G(z) \right\rangle = 0. \tag{35}$$

It is easy to solve the adjoint eigenvalue problem by employing a simple transformation as shown in Appendix B. Taking into consideration (22), the last integral of (34) is proportional to the horizontal integral of the cube of Φ (cf. Joseph 1976, Vol. 2, section 73) and thus vanishes for the two-dimensional rolls of (A 3)–(A 5). Equations (34) and (35) then reduce to

$$R_1 = \frac{|\epsilon|}{\epsilon} \omega Da \frac{\langle \boldsymbol{U}_0^* \cdot \boldsymbol{U}_0 |\boldsymbol{U}_0| \rangle}{\langle \pm w_0^* \theta_0 + G(z)\, \theta_0^*\, w_0 \rangle} = \frac{|\epsilon|}{\epsilon} \omega Da\, r_1(\eta), \tag{36}$$

$$R_2 = \frac{|\epsilon|}{\epsilon} \frac{R_0 \left\langle \theta_0^* \frac{\partial}{\partial z} |\boldsymbol{U}_0|\, G(z) \right\rangle}{\langle \pm w_0^* \theta_0 + G(z)\, \theta_0^*\, w_0 \rangle} = \frac{|\epsilon|}{\epsilon} r_2(\eta). \tag{37}$$

The ratios r_1, r_2 of (36) and (37) are evaluated via numerical integration over the domain $(y, z) = [0, \lambda] \times [0, 1]$ and the results are tabulated in tables 3 and 4; B_1 is the amplitude of the $\boldsymbol{q}_0$ vector given in (A 3)–(A 6).

The expansion (16) for the modified Rayleigh number now becomes

$$R = R_0 + |\epsilon|\, \omega Da\, r_1(\eta) + \delta \frac{|\epsilon|}{\epsilon} r_2(\eta). \tag{38}$$

Noting that $r_1(\eta)$ is always positive and that $r_2(\eta)$ has the sign of $-\Delta T$, we sketch qualitatively the bifurcation diagrams in figure 4 and make the following observations:

(i) The bifurcation curves are asymmetric with respect to ϵ and consist of two disjoint branches that originate at distances $\delta r_2(\eta)$ below and above the critical value R_0. This separation is of order d/L, so it would be easy to detect experimentally for coarse beds. This is the effect of dispersion near the first bifurcation.

(ii) Unlike the analogous Bénard problem in pure fluids with internal heat generation, the bifurcation at R_0 for the porous-medium Bénard problem is not two-sided. Moreover, it does not fall into any pitchfork class known.

(iii) Without internal heat generation, $r_2(0) = 0$, so a symmetric supercritical pitchfork bifurcation occurs. This peculiar one-sided bifurcation has been observed by Nield & Joseph (1985) and Georgiadis & Catton (1988*a*).

η	R_0	$\dfrac{R_1}{\dfrac{\lvert\epsilon\rvert}{\epsilon}\omega Da B_1}$	$\dfrac{R_2}{\dfrac{\lvert\epsilon\rvert}{\epsilon}}$
0	6.28	3.14	0.00
10	5.20	2.30	−2.51
20	4.20	1.90	−3.23
30	3.59	1.67	−3.10
40	3.19	1.50	−2.88
50	2.89	1.37	−2.68
60	2.67	1.28	−2.51
70	2.49	1.19	−2.36
80	2.34	1.13	−2.24
90	2.21	1.07	−2.13
100	2.11	1.02	−2.04

TABLE 3. The values of the coefficients of the Rayleigh-number expansion ($\Delta T > 0$)

η	R_0	$\dfrac{R_1}{\dfrac{\lvert\epsilon\rvert}{\epsilon}\omega Da B_1}$	$\dfrac{R_2}{\dfrac{\lvert\epsilon\rvert}{\epsilon}}$
10	9.70	5.26	4.74
20	5.71	3.09	5.28
30	4.41	2.33	4.38
40	3.71	1.94	3.76
50	3.27	1.69	3.32
60	2.95	1.51	3.00
70	2.71	1.38	2.76
80	2.52	1.28	2.56
90	2.37	1.20	2.40
100	2.24	1.13	2.27

TABLE 4. The values of the coefficients of the Rayleigh-number expansion ($\Delta T < 0$)

It is obvious that the two bifurcation branches represent different finite-amplitude solutions near the onset of convection with internal heat generation. The shape of bifurcation implies that a certain form of hysteresis could possibly be observed during experiments performed for the purpose of determining the critical Rayleigh number; a different critical value is obtained depending on whether ΔT approaches the critical from below or from above. We do not pursue the study of the stability of the bifurcation branches or the bifurcation characteristics of other planforms besides straight rolls in this work. Owing to the degeneracy of the spectrum, an infinite set of planforms of cellular convection is possible (but not always stable to infinitesimal disturbances) in horizontally unbounded domains.

5. Conclusions

We have studied basically the effect of first-order nonlinear extensions to the Darcy–Boussinesq model on the onset of natural convection in a porous layer. These extensions correspond to a drag coefficient and effective thermal conductivity that

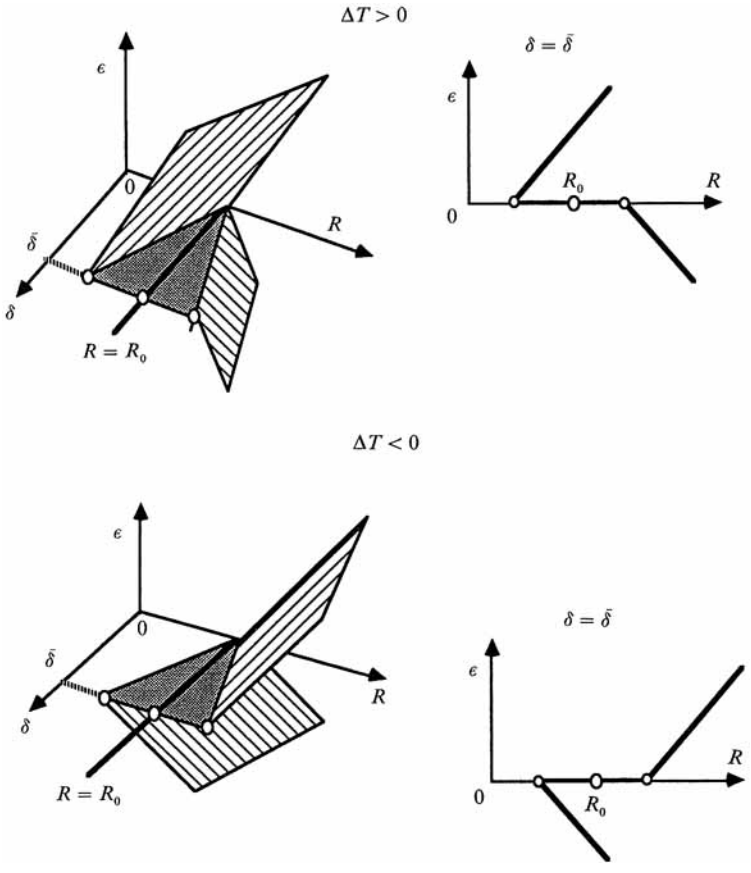

FIGURE 4. Bifurcation diagrams for the Bénard problem in a fully saturated porous layer with internal heat generation.

depend linearly on the magnitude of the local velocity vector. We have computed the neutral curves and showed that the nonlinear terms are more important than boundary effects (i.e. Brinkman extension) when internal heat generation is included. The bifurcation curves for two-dimensional stationary rolls are also calculated for different internal heat generation intensities. Unlike its pure-fluid counterpart, the porous Bénard problem exhibits an atypical bifurcation curve which does not belong to the common pitchfork class of bifurcations. The bifurcation diagram is asymmetric and has two disjoint branches that are separated by a distance proportional to the dispersivity (which is proportional to d/L). The stability characteristics of the bifurcation branches and the calculation of bifurcation curves for other planforms (e.g. hexagons) is beyond the scope of the present investigation.

In view of the scatter in critical Rayleigh numbers reported in experimental investigations of related problems, our model can potentially supplement studies of the effects of small imperfections on bifurcation. Such studies focus typically on the effect of boundary imperfections on the Darcy model (Rees & Riley 1986, 1989). The ultimate test of our formulation and of the predicted uncommon bifurcation curve, in particular, will come as a result of a direct experimental investigation of the porous Bénard problem with isothermal boundaries and internal heat generation.

This work is supported by the Engineering Foundation under Research Initiation Grant RI-A-88-9 and by the National Science Foundation under grand CTS-8909119. The authors wish to acknowledge the helpful comments by Professor Ivan Catton of the University of California at Los Angeles and Professor Donald Nield of the University of Auckland.

Appendix A

The vectors, matrices and operators in equations (17)–(19) are given by

$$\left.\begin{gathered}\boldsymbol{D}^{\mathrm{T}} = -Da\left(\frac{\partial}{\partial x}, \frac{\partial}{\partial y}, \frac{\partial}{\partial z}, 0\right), \quad \boldsymbol{q}_i = (u_i, v_i, w_i, \theta_i)^{\mathrm{T}}, \quad \boldsymbol{I} = (1,1,1,1)^{\mathrm{T}}, \\ \boldsymbol{L}_{00} = -\begin{bmatrix} -1 & 0 & 0 & 0 \\ 0 & -1 & 0 & 0 \\ 0 & 0 & -1 & \pm R_0 \\ 0 & 0 & R_0 G(z) & \nabla^2 \end{bmatrix}, \quad \boldsymbol{L}_{10} = -\begin{bmatrix} 0 & 0 & 0 & 0 \\ 0 & 0 & 0 & 0 \\ 0 & 0 & 0 & \pm R_1 \\ 0 & 0 & R_1 G(z) & 0 \end{bmatrix} \\ \boldsymbol{L}_{20} = -\begin{bmatrix} 0 & 0 & 0 & 0 \\ 0 & 0 & 0 & 0 \\ 0 & 0 & 0 & \pm R_2 \\ 0 & 0 & R_2 G(z) & 0 \end{bmatrix}, \quad \boldsymbol{M}_{00} = \begin{bmatrix} 0 & 0 & 0 & 0 \\ 0 & 0 & 0 & 0 \\ 0 & 0 & 0 & 0 \\ 0 & 0 & 0 & \boldsymbol{U}_0 \cdot \nabla \end{bmatrix} \\ \boldsymbol{N}_{00} = \frac{|\epsilon|}{\epsilon} \omega Da |\boldsymbol{U}_0| \begin{bmatrix} 1 & 0 & 0 & 0 \\ 0 & 1 & 0 & 0 \\ 0 & 0 & 1 & 0 \\ 0 & 0 & 0 & 0 \end{bmatrix}, \quad \boldsymbol{F}_{00} = \frac{|\epsilon|}{\epsilon} R_0 \frac{\partial}{\partial z}[|\boldsymbol{U}_0| G(z)] \begin{bmatrix} 0 & 0 & 0 & 0 \\ 0 & 0 & 0 & 0 \\ 0 & 0 & 0 & 0 \\ 0 & 0 & 0 & 1 \end{bmatrix}\end{gathered}\right\} \tag{A 1}$$

The integrals of (31) are defined as

$$I_0^{mn} = \int_0^1 G(z) \sin(m\pi z) \sin(n\pi z)\, \mathrm{d}z, \quad I_1^{mn} = \int_0^1 \sin(m\pi z) \sin(n\pi z)\, \mathrm{d}z. \tag{A 2}$$

Hence,

$$\begin{aligned} I_0^{mn} &= 0 && \text{if } m-n \text{ even}, \\ I_0^{mn} &= \frac{-4\eta mn}{\pi^2(m^2-n^2)^2} && \text{if } m-n \text{ odd}, \\ I_0^{mn} &= \tfrac{1}{2} && \text{if } m = n, \\ I_1^{mn} &= \tfrac{1}{2} && \text{if } m = n, \\ I_1^{mn} &= 0 && \text{if } m \neq n. \end{aligned}$$

The eigenfunctions of (20) and (21) for two-dimensional cellular convection are given by

$$v_0 = -\frac{\pi}{\alpha} \sin(\alpha y)\,[B_1 \cos(\pi z) + 2B_2 \cos(2\pi z) + 3B_3 \cos(3\pi z)], \tag{A 3}$$

$$w_0 = \cos(\alpha y)\,[B_1 \sin(\pi z) + B_2 \sin(2\pi z) + B_3 \sin(3\pi z)], \tag{A 4}$$

$$\theta_0 = \frac{1}{\pm R_0 \alpha^2} \cos(\alpha y)\,[B_1(\pi^2+\alpha^2) \sin(\pi z) + B_2(4\pi^2+\alpha^2) \sin(2\pi z) + B_3(9\pi^2+\alpha^2) \sin(3\pi z)], \tag{A 5}$$

where $$B_2 = B_1 \frac{9\pi^2[\pm\alpha^2 R_0^2 - (\pi^2+\alpha^2)^2]}{\pm 16\eta R_0^2 \alpha^2}, \quad B_3 = \tfrac{27}{25} B_1 \frac{\pm\alpha^2 R_0^2 - (\pi^2+\alpha^2)^2}{\pm\alpha^2 R_0^2 - (9\pi^2+\alpha^2)^2}. \tag{A 6}$$

Appendix B

The adjoint eigenvalue problem to (20) and (21) is obtained with the transpose $\boldsymbol{L}_{00}^{\mathrm{T}}$

$$-\nabla^2 w_0^* + R_0 G(z) \nabla_1^2 \theta_0^* = 0, \tag{B 1}$$

$$\pm R_0 w_0^* + \nabla^2 \theta_0^* = 0. \tag{B 2}$$

The adjoint problem has the same eigenvalues $R_0(\alpha)$ as (20) and (21) and can be solved with separation of variables as in (22):

$$\begin{bmatrix} w_0^* \\ \theta_0^* \end{bmatrix} = \begin{bmatrix} W_0^*(z) \\ \Theta_0^*(z) \end{bmatrix} \Phi(x, y) \tag{B 3}$$

where $\Phi(x, y)$ is the planform function given by (23). Comparing the systems (20) and (21) and (B 1) and (B 2), we can make the following observations: (i) If $G(z) = 1$ ($\eta = 0$, no internal heating), only the unstably heated layer becomes unstable, and $\boldsymbol{L}_{00}$ is self-adjoint. (ii) By making the substitutions

$$w_0^* = \alpha^2 \theta_0, \quad \theta_0^* = w_0 \tag{B 4}$$

we recover the eigenvalue problem (20) and (21). This implies that (B 4) gives the adjoint eigenfunctions.

REFERENCES

Buretta, R. J. & Berman, A. S. 1976 Convective heat transfer in a liquid saturated porous layer. *Trans. ASME* E: *J. Appl. Mech.* **98**, 249–253.

Close, D. G., Symmons, J. G. & White, R. F. 1985 Convective heat transfer in shallow, gas-filled porous media: experimental investigation. *Intl J. Heat Mass Transfer* **28**, 2371–2378.

Ergun, S. 1952 Fluid flow through packed columns. *Chem. Engng Prog.* **48**, 89–94.

Gartling, D. K. & Hickox, C. E. 1985 Numerical study of the application of the Boussinesq approximation for a fluid-saturated porous medium. *Intl J. Numer. Meth. Fluids* **5**, 995–1013.

Gasser, R. D. & Kazimi, M. S. 1976 Onset of convection in a porous medium with internal heat generation. *Trans. ASME* C: *J. Heat Transfer* **98**, 49–54.

Georgiadis, J. G & Catton, I. 1987 Stochastic modeling of unidirectional fluid transport in uniform and random packed beds. *Phys. Fluids* **30**, 1017–1022.

Georgiadis, J. G & Catton, I. 1988*a* An effective equation governing convective transport in porous media. *Trans. ASME* C: *J. Heat Transfer* **110**, 635–641.

Georgiadis, J. G & Catton, I. 1988*b* Dispersion in cellular thermal convection in porous media. *Intl. J. Heat Mass Transfer* **31**, 1081–1091.

Hardee, H. C. & Nilson, R. H. 1977 Natural convection in porous media with heat generation. *Intl J. Heat Mass Transfer* **63**, 119–132.

Hwang, I. 1971 Finite amplitude thermal convection in porous media with heat source and variable viscosity. Ph.D. thesis, University of Minnesota.

Joseph, D. D. 1976 *Stability of Fluid Motions*, Vols. 1 and 2. Springer.

Katto, Y. & Masuoka, T. 1967 Criterion for the onset of convection in a fluid in a porous medium. *Intl J. Heat Mass Transfer* **10**, 296–309.

Koch, D. & Brady, J. F. 1985 Dispersion in fixed beds. *J. Fluid Mech.* **154**, 399–427.

Koch, D., Cox, R., Brenner, H. & Brady, J. F. 1989 The effect of order on dispersion in porous media. *J. Fluid Mech.* **200**, 173–188.

Kulacki, F. A. & Freeman, R. G. 1979 A note on thermal convection in a saturated, heat-generating porous layer. *Trans. ASME* C: *J. Heat Transfer* **101**, 169–171.

KVERNVOLD, O. & TYVAND, P. 1980 Dispersion effects on thermal convection in porous media. *J. Fluid Mech.* **99**, 673–686.

LEVEC, J. & CARBONELL, R. G. 1985 Longitudinal and lateral thermal dispersion in packed beds – Part II: comparison between theory and experiment, *AIChE J.* **31**, 591–602.

NEISCHLOSS, H. & DAGAN, G. 1975 Convective currence in a porous layer heated from below: The influence of hydrodynamic dispersion. *Phys. Fluids* **18**, 757–761.

NIELD, D. A. & JOSEPH, D. D. 1985 Effects of quadratic drag on convection in a saturated porous medium. *Phys. Fluids* **28**, 995–997.

REES, D. A. S. & RILEY, D. S. 1986 Free convection in an undulating saturated porous layer: resonant wavelength excitation. *J. Fluid Mech.* **166**, 503–530.

REES, D. A. S. & RILEY, D. S. 1989 The effects of boundary imperfections on convection in a saturated porous layer: near-resonant wavelength excitation. *J. Fluid Mech.* **199**, 133–154.

RHEE, S. J., DHIR, V. K. & CATTON, I. 1978 Natural convection heat transfer in beds of inductively heated particles. *Trans. ASME* C: *J. Heat Transfer* **100**, 78–85.

RUBIN, H. 1974 Heat dispersion effect on thermal convection in a porous medium layer. *J. Hydrol.* **21**, 173–185.

RUDRAIAH, N., VERRAPPA, B. & BALACHANDRA, R. 1982 Convection in a fluid-saturated porous layer with non-uniform temperature gradient. *Intl J. Heat Mass Transfer* **25**, 1147–1156.

SELIMOS, B. & POULIKAKOS, D. 1985 On double diffusion in a Brinkman heat generating porous layer. *Intl Commun. Heat Mass Transfer* **12**, 149–158.